

1 **Long-term variations in solar wind parameters,**
2 **magnetopause location, and geomagnetic activity over**
3 **the last five solar cycles**

4 **A. A. Samsonov¹, Y. V. Bogdanova², G. Branduardi-Raymont¹, J.**
5 **Safrankova³, Z. Nemecek³, and J.-S. Park⁴**

6 ¹Mullard Space Science Laboratory, University College London, UK

7 ²RAL Space, Rutherford Appleton Laboratory, Science and Technology Facilities Council, UK

8 ³Charles University, Prague, Czech Republic

9 ⁴Shandong Provincial Key Laboratory of Optical Astronomy and Solar-Terrestrial Environment, Institute
10 of Space Sciences, Shandong University, Weihai, China

11 **Key Points:**

- 12 • Average annual magnetopause standoff distance increased by nearly $2 R_E$ from
13 1991 to 2009
- 14 • Solar wind dynamic pressure anticorrelates with sunspot number in cycles 20-21
15 and correlates in cycles 22-24
- 16 • The best correlation between annual solar wind dynamic pressure and sunspot num-
17 ber was found for 2-3 year delay

Corresponding author: Andrey Samsonov, a.samsonov@ucl.ac.uk

18 **Abstract**

19 We use both solar wind observations and empirical magnetopause models to recon-
 20 struct time series of the magnetopause standoff distance for nearly five solar cycles. Since
 21 the average annual interplanetary magnetic field (IMF) B_z is about zero, and the an-
 22 nual IMF cone angle varies between 54.0° and 61.2° , the magnetopause standoff distance
 23 on this time scale depends mostly on the solar wind dynamic pressure. The annual IMF
 24 magnitude well correlates with the sunspot number (SSN) with a zero time lag, while
 25 the annual solar wind dynamic pressure (P_{dyn}) correlates reasonably well with the SSN
 26 but with 3 years time lag. At the same time, we find an anticorrelation between P_{dyn}
 27 and SSN in cycles 20–21 and a correlation in cycles 22–24 with 2 years time lag. Both
 28 the annual solar wind density and velocity well correlate with the dynamic pressure, but
 29 the correlation coefficient is higher for density than for velocity. The 11-year solar cy-
 30 cles in the dynamic pressure variations are superimposed by an increasing trend before
 31 1991 and a decreasing trend between 1991 and 2009. The average annual solar wind dy-
 32 namic pressure decreases by a factor of three from 1991 to 2009. Correspondingly, the
 33 predicted standoff distance in Lin et al.’s (2010) magnetopause model increases from 9.7
 34 R_E in 1991 to 11.6 R_E in 2009. The annual SSN, IMF magnitude and magnetospheric
 35 geomagnetic activity indices display the same trends as the dynamic pressure. We cal-
 36 culate extreme solar wind parameters and magnetopause standoff distance in each year
 37 using daily values and find that both extremely small and large standoff distances dur-
 38 ing a solar cycle preferably occur at solar maximum rather than at solar minimum.

39 **1 Introduction**

40 Periodic variations of the coronal magnetic field (solar cycles) are synchronized with
 41 many processes in the geospace environment. Besides the well-known 11-year solar cy-
 42 cles, longer solar periodicities have also been revealed in the ground data. In particu-
 43 lar, the studies of auroral records show variations with a mean period of about 80-90 years
 44 (Link, 1962; Gleissberg, 1965; Siscoe, 1980) often referred to as the Gleissberg cycle. The
 45 solar variations are transported to the Earth through the solar wind, solar energetic par-
 46 ticles, and solar radiation. The 11-year periodicity has been observed in most solar wind
 47 parameters, such as the interplanetary magnetic field (IMF) magnitude (King, 1979),
 48 the IMF $|B_z|$ (Siscoe et al., 1978), and the helium content (Neugebauer, 1981; Aellig et
 49 al., 2001) almost from the start of the space era. A similar periodicity was found in the
 50 solar wind plasma parameters, e.g. density and velocity (Dmitriev et al., 2009).

51 However, the cycles of solar wind parameters and indices of geomagnetic activity
 52 might not have the same phase or shape as the sunspot cycle (Hirshberg, 1973; Feyn-
 53 man, 1982). In particular, Echer et al. (2004) reported about an average one-year time
 54 lag between the time series of the geomagnetic aa index and sunspot numbers (SSN) us-
 55 ing correlation analysis for the period of 1868-2000. At the same time, the authors noted
 56 that the time lag varied during the time interval. Gonzalez et al. (1990) observed a dual-
 57 peak solar cycle distribution of intense geomagnetic storms, with first peak occurring at
 58 the late ascending phase of the cycle or at solar maximum and second peak at the early
 59 descending phase of the cycle. The solar phenomena responsible for geomagnetic storms
 60 are Coronal Mass Ejections (CMEs) and Corotating Interaction Regions (CIRs). The
 61 occurrence rate of CMEs peaks during solar maximum, while the occurrence rate of CIRs
 62 peaks during the declining phase of the solar cycle (Borovsky & Denton, 2006, and ref-
 63 erences therein). Bothmer and the EU-INTAS-ESA Team (2004) noted that CIRs may
 64 play a role also during the rising phase. In general, however, the CME-driven storms mostly
 65 occur near solar maximum, and the CIR-driven storms mostly occur in the declining phase.

66 Several papers studied long-term variations in the solar wind velocity and the open
 67 solar magnetic flux by making reconstruction of the velocity from the geomagnetic in-
 68 dices (Lockwood et al., 2009; Rouillard et al., 2007). They mostly used the aa index be-

69 cause the time series for aa is longer than for other geomagnetic indices. According to
 70 Lockwood et al. (2009), the reconstructed annual solar wind velocity varied nearly from
 71 300 to 550 km/s during the twentieth century. The averaged solar wind velocity and IMF
 72 magnitude obtained from in-situ data between 1965 and 2010 were presented and dis-
 73 cussed by Zerbo et al. (2013). This study also indicated significant variations in the so-
 74 lar wind speed which generally match the variations in the aa index. Dmitriev et al. (2005,
 75 2009) analyzed solar wind plasma and magnetic field properties during four solar cycles
 76 from 20th to 23rd. In particular, Dmitriev et al. (2009) obtained the periodicity and dis-
 77 tribution functions for several dimensional and dimensionless parameters. They showed
 78 that the statistical distributions of both IMF magnitude and solar wind density are close
 79 to a lognormal distribution function, while the velocity distribution is different from a
 80 lognormal one. This reflects the observational fact that the relative dispersion of aver-
 81 age solar wind velocity is smaller than the relative dispersion of IMF magnitude or so-
 82 lar wind density.

83 The last (24th) solar cycle has the lowest sunspot activity since the Dalton min-
 84 imum (early 1800s). Janardhan et al. (2015) reported that the solar photospheric fields
 85 at high latitudes have been steadily declining since 1995. McComas et al. (2013) com-
 86 pared average solar wind parameters observed from the mid-1970s through the mid-1990s
 87 and from 2009 through the beginning of 2013. They showed a significant decrease in the
 88 proton temperature, mass and momentum fluxes, and IMF magnitude in the last solar
 89 cycle and noted that these results may have important implication for the solar wind in-
 90 teraction with planetary magnetospheres. Similar results were obtained by Zerbo and
 91 Richardson (2015) who noted that the solar wind magnetic field, speed, and density re-
 92 mained anomalously low from the 23rd solar minimum to the 24th solar maximum. The
 93 weak solar activity and small IMF result in decrease of the geomagnetic activity at the
 94 same time. Kilpua et al. (2014) examined the geomagnetic activity using Dst and AE
 95 indices, the solar wind conditions, and the occurrence rate of interplanetary coronal mass
 96 ejections (ICME) during two periods, from 1995 to 1999 and from 2006 to 2012. They
 97 concluded that the geomagnetic activity was considerably weaker during the second time
 98 interval, in particular in terms of Dst , and related this mainly to a weaker southward IMF
 99 component.

100 The variations of solar wind parameters, such as the velocity and B_z magnitude,
 101 modulate the solar wind energy input into the magnetosphere through the variations of
 102 the reconnection rate at the dayside magnetopause. Besides, another consequence of vari-
 103 ations in the solar wind parameters might be variable magnetospheric compression. Petr-
 104 netec et al. (1991) used 10 years ISEE data from 1977 to 1987 to study variations of the mag-
 105 netopause size and shape with the solar wind data. Surprisingly, they found that the so-
 106 lar wind dynamic pressure was the lowest values at solar maximum, in the 1979-1980 sea-
 107 son, and the dynamic pressure had largest values, more than double the value in 1979-
 108 1980, at the following solar minimum. According to most magnetopause models, the mag-
 109 netopause standoff distance depends both on the solar wind dynamic pressure and IMF
 110 B_z . Since there are no continuous observations at the dayside magnetopause, the vari-
 111 ations of magnetopause position during a solar cycle may be difficult to detect directly
 112 using in situ observations. However, Petrnetec et al. (1991) concluded that the average
 113 size of the magnetosphere varies significantly throughout the course of the solar cycle
 114 for both northward and southward IMF orientations. In agreement with the variations
 115 of the dynamic pressure, the standoff magnetopause distance was largest near solar max-
 116 imum. Richardson et al. (2000) studied the same solar maximum of cycle 21 using so-
 117 lar wind data and geomagnetic aa index and showed both a temporal reduction in av-
 118 erage solar wind speed and IMF magnitude and an associated depression in aa index in
 119 1980. Dmitriev et al. (2005) also noted drops of the solar wind dynamic pressure and
 120 flux density near solar maxima, especially in cycles 20 and 21.

121 To our knowledge, the long-term variations in the magnetopause size have not been
 122 studied so far, except for the above-mentioned work of Petrinec et al. (1991) in which
 123 only a relatively short time interval was investigated. At present, in situ solar wind data
 124 referred to the bow shock nose are available in the OMNIWeb database for almost five
 125 solar cycle. Besides, many empirical magnetopause models have been developed in or-
 126 der to predict the standoff distance as a function of the solar wind input parameters (Dmitriev
 127 et al., 2011; Kuznetsov & Suvorova, 1998; Lin et al., 2010; Petrinec & Russell, 1996; Pu-
 128 dovkin et al., 1998; Roelof & Sibeck, 1993; Shue et al., 1998). Despite some quantita-
 129 tive discrepancies in model predictions (Samsonov et al., 2016), they mostly use the same
 130 expressions connecting the solar wind dynamic pressure with the standoff distance. It
 131 is also known (and will be demonstrated again below) that the average IMF B_z on the
 132 time scale of months or years is approaching zero (see, e.g., Dmitriev et al. (2009)), there-
 133 fore we believe that the dynamic pressure is the main factor which determines the long-
 134 term variations in the magnetopause size.

135 Recent studies have pointed out that during intervals with a nearly radial IMF ori-
 136 entation, the dayside magnetopause expands (Dušík et al., 2010; Grygorov et al., 2017;
 137 Jelínek et al., 2010; Merka et al., 2003; Park et al., 2016) due to a significant decrease
 138 in the total pressure in the magnetosheath (Samsonov et al., 2012; Suvorova et al., 2010).
 139 In some exceptional cases, such time intervals may last several hours, and this may shift
 140 the magnetopause position about 1-2 R_E outward (Samsonov et al., 2017). The mag-
 141 netopause models have not taken into account this effect so far, nevertheless we discuss
 142 the influence of quasi-radial IMF intervals on our results below.

143 The main motivation of this work is to investigate how the average magnetopause
 144 size has varied in the space era using OMNI data and empirical magnetopause models.
 145 We do not limit our attention only to variations in the solar wind dynamic pressure, but
 146 also explore variations in the IMF B_z and $|B|$, and in the geomagnetic indices search-
 147 ing for similar long-term trends. In addition to the study of average annual values, we
 148 consider variations in the extreme annual solar wind values and the extreme standoff dis-
 149 tance. We highlight several events when our method predicts the extreme standoff dis-
 150 tance and discuss them.

151 During very strong magnetospheric compressions, geosynchronous orbits may partly
 152 leave the magnetosphere and cross the magnetosheath or solar wind (such events are called
 153 geosynchronous magnetopause crossings, or GMCs). GMCs require sufficiently high dy-
 154 namic pressures because the effects of negative IMF B_z are saturated (Suvorova et al.,
 155 2005). GMCs may cause a significant damage to the geosynchronous spacecraft, there-
 156 fore predictions of such events are an important space weather problem (Dmitriev et al.,
 157 2014; Dmitriev et al., 2016). In this work, we estimate the range of variations in the ex-
 158 treme annual magnetopause distance during the last five solar cycles using empirical mag-
 159 netopause models.

160 The main reason of strong magnetospheric compression is a high solar wind dynamic
 161 pressure which is usually associated with a high solar wind speed. The intervals of high
 162 speed in the solar wind are associated both with CMEs and CIRs, however, an extremely
 163 high speed (e.g., $V_{SW} > 1000$ km/s) is usually related to CMEs (Gopalswamy, 2006,
 164 2008; Yashiro et al., 2004). Consequently, extremely strong magnetic storms (in terms
 165 of the Dst index) are mostly CME-driven (Gosling et al., 1990; Borovsky & Denton, 2006;
 166 Denton et al., 2006). Strong storms sometimes result from the interaction between two
 167 successive CMEs or a CME and a high speed stream (Liu et al., 2015; Lugaz et al., 2017).
 168 Oh et al. (2007) concluded that CMEs (or more precisely magnetic clouds) are also the
 169 most dominant and strong driver of interplanetary shocks. We suggest below that strong
 170 CMEs or sequences of CMEs result in events with extremely strong magnetospheric com-
 171 pression.

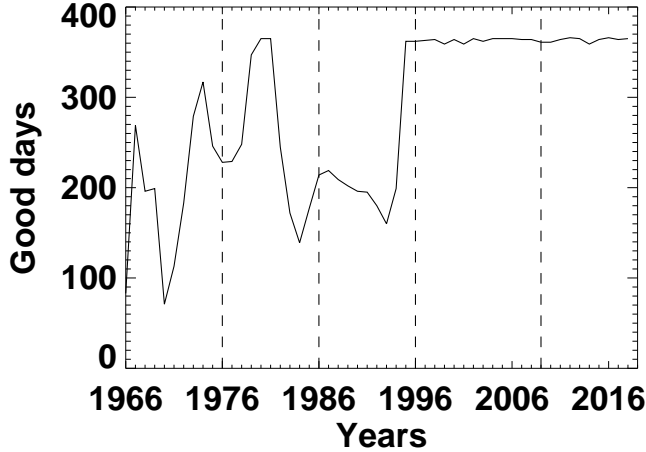


Figure 1. The number of days in each year which we have used for finding average annual values.

172 Besides the solar wind velocity, the dynamic pressure depends also on the solar wind
 173 density, and both CMEs and CIRs are usually accompanied by a density increase. We
 174 discuss below the correlations between the annual density, velocity and dynamic pres-
 175 sure.

176 The paper is organized as follows. In section 2, we show and discuss the average
 177 and extreme solar wind and magnetospheric parameters over the last five solar cycles.
 178 In section 3, we investigate events when the magnetosphere is extremely compressed. We
 179 close the paper with discussion and conclusions.

180 **2 Solar wind and magnetospheric cycles and trends**

181 We begin this study with the hourly average solar wind parameters from OMNI
 182 (omniweb.gsfc.nasa.gov) and find the daily average values. Later, we use these daily av-
 183 erages when finding maximal and minimal extreme values for each year (we call them
 184 *extreme annual values* below). On the next step, we calculate both the monthly and an-
 185 nual average values from the daily averages. The OMNI database contains solar wind
 186 parameters from 1964, but the data in 1964 and 1965 have many gaps, therefore we con-
 187 sider only the time interval from 1966 to 2018. However, the OMNI data still contain
 188 a lot of data gaps before 1995 (Lockwood et al., 2019). We exclude daily averages from
 189 the processing if they contain less than 8 hourly average solar wind values, either in mag-
 190 netic field or in plasma data. Figure 1 shows the number of "good" days, i.e. the days
 191 which can be used to find the averages for each year. We have tried different minimum
 192 threshold conditions demanding from 5 to 12 hours of good data for each day and found
 193 that the averages are slightly changed only before 1995, and that this does not change
 194 the conclusions of the paper. Thus, the considered time interval covers completely three
 195 solar cycles (21-23) and almost completely the 20th and 24th cycles, so nearly 5 cycles
 196 in total.

197 For a given solar wind dynamic pressure and IMF, we calculate the magnetopause
 198 standoff distance using Shue et al.'s (S98) and Lin et al.'s (L10) magnetopause models.
 199 We use the magnetospheric Dst and Kp indices for illustration of the magnetospheric
 200 response to solar wind variations. The Dst index reflects the variations in the ring cur-
 201 rent, magnetopause current, and partly in the tail current (Burton et al., 1975). We will
 202 use $-Dst$ throughout the paper because increase in the geomagnetic activity actually

203 means decrease in Dst . The Kp index indicates the level of overall magnetospheric dis-
 204 turbance.

205 Figure 2 shows the annual sunspot numbers (SSN), average and extreme IMF mag-
 206 nitude and B_z (we use GSM coordinates here and below), IMF cone angle (the angle be-
 207 tween IMF vector and x axis, i.e. $\arccos(|B_x|/|B|)$), solar wind dynamic pressure P_{dyn}
 208 and velocity, magnetopause standoff distance, and $-Dst$ index. We discuss first the ex-
 209 tremes annual solar wind values shown by red and blue lines in Figure 2. The maximum
 210 $|B|$, maximum and minimum B_z , maximum dynamic pressure, and finally maximum so-
 211 lar wind velocity in general display the 11-year cycle similar to the SSN, although with
 212 large fluctuations. The two exceptions are cycle 20 when both the maximum $|B|$ and max-
 213 imum P_{dyn} (and V) do not reveal any increase near solar maximum, and cycle 21, in
 214 which a great increase of maximum P_{dyn} occurs at the beginning of the cycle, in 1976-
 215 1977. The average annual dynamic pressure (shown in both Figures 2 and 4) in cycles
 216 20-21 exhibits the same trends as the maximum P_{dyn} . Considering these two cycles, Crooker
 217 and Gringauz (1993) concluded that the dynamic pressure anticorrelates with the SSN,
 218 but we do not confirm this conclusion when analyzing the whole 5-cycle interval.

219 Since the extreme values in Figure 2 are obtained from daily averages (one extreme
 220 value for each year), we believe that they probably correspond to the strongest coronal
 221 mass ejections (CME) in each year reaching the Earth. Note that the date with extreme
 222 conditions for one parameter (e.g., for $|B|$) usually does not coincide with the date with
 223 extreme conditions for another parameter (e.g., P_{dyn}). However, the solar wind condi-
 224 tions for a whole day whether with a strong dynamic pressure, e.g. on average higher
 225 than 10 nPa, or with a high negative B_z , e.g. about -10 nT or lower, result in signifi-
 226 cant magnetospheric disturbances, possibly commencing magnetic storms.

227 Increase in the solar wind dynamic pressure results in decrease in the minimum mag-
 228 netopause standoff distance as shown by blue lines on the 7th panel from the top of Fig-
 229 ure 2. Both S98 and L10 models predict the smallest daily standoff distance in the mid-
 230 dle of the 22nd cycle, in 1991, when the standoff distance decreased to $5.9 R_E$ (see Ta-
 231 ble 3 below). Interestingly, the variations in the maximum standoff distance also roughly
 232 follow the solar cycles. The peaks in the maximum standoff distance which correspond
 233 to the deepest minima of the dynamic pressure are located mainly in the middle of so-
 234 lar cycles, although the correlation between maximum R_{sub} and SSN is poor. In other
 235 words, the probability of getting an extremely small dynamic pressure seems to be higher
 236 near solar maximum than near solar minimum too. This is also the case for the extremely
 237 large dynamic pressure. The correlation between the maximum annual dynamic pres-
 238 sure and the annual SSN is statistically significant with the coefficient of 0.364.

239 Comparing the results of S98 (solid) and L10 (dashed) magnetopause models, we
 240 conclude that both models predict qualitatively very similar variations (since they are
 241 determined by dynamic pressure in both cases), but the L10 model usually predicts slightly
 242 larger maximum or smaller minimum standoff distance. The reason for this is that the
 243 L10 model implies a stronger dependence of the standoff distance on the dynamic pres-
 244 sure ($R_{S98} \sim P_{dyn}^{-0.15}$, while $R_{L10} \sim (P_{dyn} + P_m)^{-0.19}$, here P_m is magnetic pres-
 245 sure). The maximum Dst index also displays the 11-year cycle as expected.

246 After emphasizing the extreme solar wind parameters in Figure 2, we now consider
 247 the solar cycles and long-term trends in the average annual values. Figure 4 shows the
 248 annual SSN, IMF magnitude and average southward IMF, IMF cone angle, solar wind
 249 dynamic pressure, magnetopause standoff distance, Kp and $-Dst$ indices. The average
 250 southward component B_s has been obtained from hourly B_z such that $B_s = 0$ for $B_z >$
 251 0 and $B_s = -B_z$ for $B_z < 0$. Both the average $|B|$ and B_s clearly vary with the 11-
 252 year periodicity, except may be during the 20th cycle. Note that the number of days with
 253 data gaps in the 20th cycle is larger than in the following cycles which might explain the
 254 different behavior of the average parameters in this cycle. At the same time, magneto-

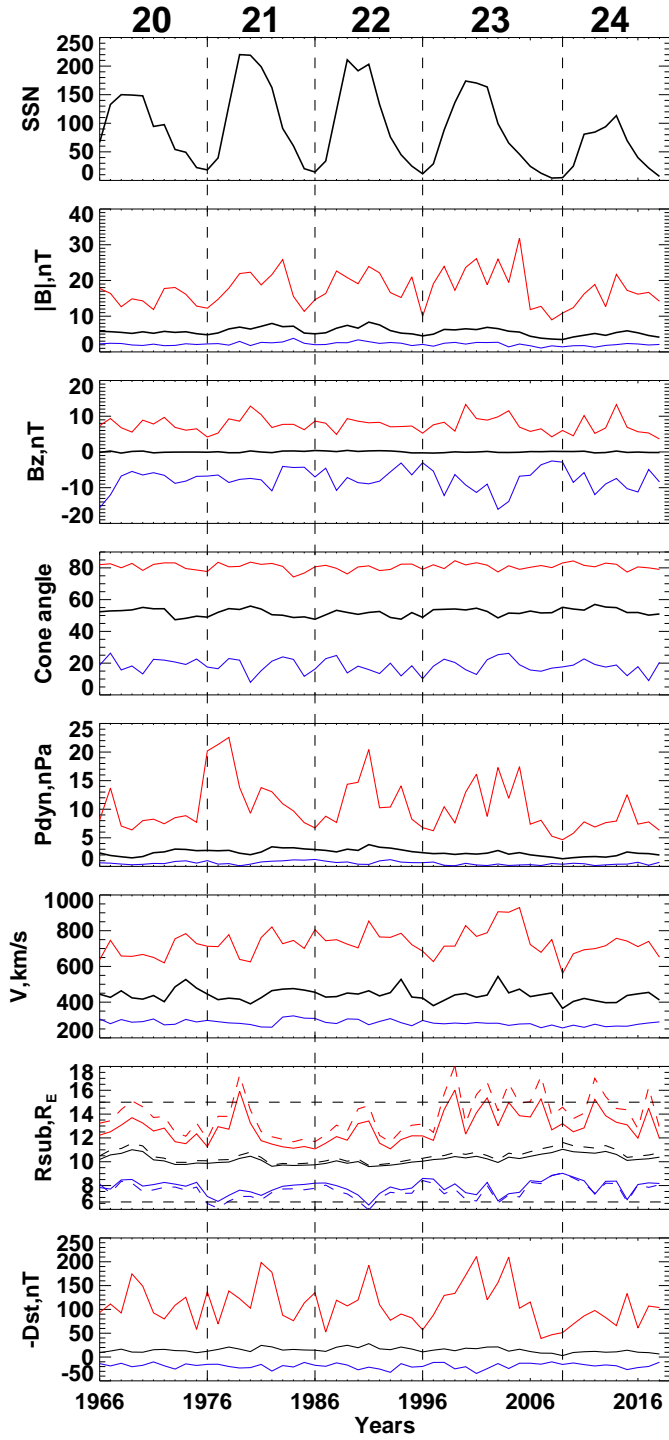


Figure 2. The sunspot numbers (average daily number for each year), average and extreme IMF magnitude and B_z , IMF cone angle (the angle between IMF vector and x axis), solar wind dynamic pressure and velocity, magnetopause standoff distance (solid lines for Shue et al.'s model and dashed lines for Lin et al.'s model), and geomagnetic $-Dst$ index. Annual average values shown by black, daily maximal and minimal values for each year shown by red and blue. Vertical lines separate solar cycles as indicated by numbers at the top.

Table 1. Pearson correlation coefficients for annual sunspot numbers, solar wind parameters, magnetopause distance calculated by L10 model, and magnetospheric indices for a zero time lag between all parameters. Letter N instead of some correlation coefficients indicates that the correlation between these parameters is not statistically significant. The correlation between SSN and P_{dyn} (R_{sub}) increases for a non-zero time lag (see explanation in text and Figure 4 below). All correlation coefficients for Dst are negative because Dst becomes stronger negative for more disturbed magnetospheric conditions.

	SSN	$ B $	B_s	θ	N	V	P_{dyn}	R_{sub}	Kp	Dst
SSN	1.000	0.748	0.784	0.301	N	N	N	N	0.435	-0.611
$ B $	0.748	1.000	0.833	N	0.339	0.321	0.665	-0.588	0.836	-0.808
B_s	0.784	0.833	1.000	N	N	N	0.340	-0.301	0.584	-0.714
θ	0.301	N	N	1.000	-0.512	-0.608	-0.718	0.748	-0.514	N
N	N	0.339	N	-0.512	1.000	N	0.763	-0.792	0.359	-0.371
V	N	0.321	N	-0.608	N	1.000	0.553	-0.543	0.715	-0.346
P_{dyn}	N	0.665	0.340	-0.718	0.763	0.553	1.000	-0.976	0.828	-0.628
R_{sub}	N	-0.588	-0.301	0.748	-0.792	-0.543	-0.976	1.000	-0.793	0.582
Kp	0.435	0.836	0.584	-0.514	0.359	0.715	0.828	-0.793	1.000	-0.744
Dst	-0.611	-0.808	-0.714	N	-0.371	-0.346	-0.628	0.582	-0.744	1.000

255 spheric indices in the 20th cycle also do not clearly match the solar cycle variations as
 256 they usually do, therefore the reason of unexpected variations in solar wind parameters
 257 in this cycle may be physical and is related to solar wind formation near the Sun.

258 According to Figure 4, the annual dynamic pressure exhibits slight correlation with
 259 the SSN (see discussion below), and even its annual plot displays several spikes in the
 260 whole 5-cycle interval. We suggest that the spikes of P_{dyn} are related to strong CMEs
 261 or to pairs of CME-CME and CIR-CME (Lugaz et al., 2017), which usually concentrate
 262 near solar maximum and in the declining phase.

263 We quantify the correlations in Figure 4 by finding the Pearson correlation coef-
 264 ficients (Press et al., 1992) presented in Table 1. We show only the correlation coefficients
 265 for which p-values < 0.05 , i.e. the correlation is statistically significant. The table demon-
 266 strates that the SSN well correlates with the IMF (the correlation coefficient r is 0.75
 267 for $|B|$ and 0.78 for B_s), but does not correlate with both the solar wind density and ve-
 268 locity (and correspondingly with the dynamic pressure). The IMF cone angle weakly cor-
 269 relates with the SSN ($r = 0.30$), does not correlate with the IMF magnitude and B_s , but
 270 correlates reasonably well with the density ($r = -0.51$) and velocity ($r = -0.61$). The den-
 271 sity and velocity do not correlate with each other, but both correlate with the dynamic
 272 pressure, and the correlation coefficient is higher for density ($r = 0.76$) than for veloc-
 273 ity ($r = 0.55$). The magnetopause distance calculated by the L10 model anticorrelates
 274 extremely well with the dynamic pressure as expected. It is interesting to note that Kp
 275 better correlates with P_{dyn} and V , and Dst better correlates with B_s , however both
 276 indices correlate well with $|B|$. As a result, the magnetopause distance is also better cor-
 277 related with Kp ($r = -0.79$) than with Dst ($r = 0.58$). Finally, Dst better correlates with
 278 SSN ($r = -0.61$) than Kp ($r = 0.43$).

279 Previous studies showed (Luhmann et al., 2009) that high speed solar wind streams
 280 mostly occur in the declining phases of solar cycles, therefore we have correlated the SSN
 281 and P_{dyn} with variable time lag from 1 to 11 years. Indeed the correlation coefficient
 282 between the two parameters significantly increases: we obtain maximum correlation co-
 283 efficient of 0.57 for the whole time series taking 3 years time lag, and 0.68 for only the

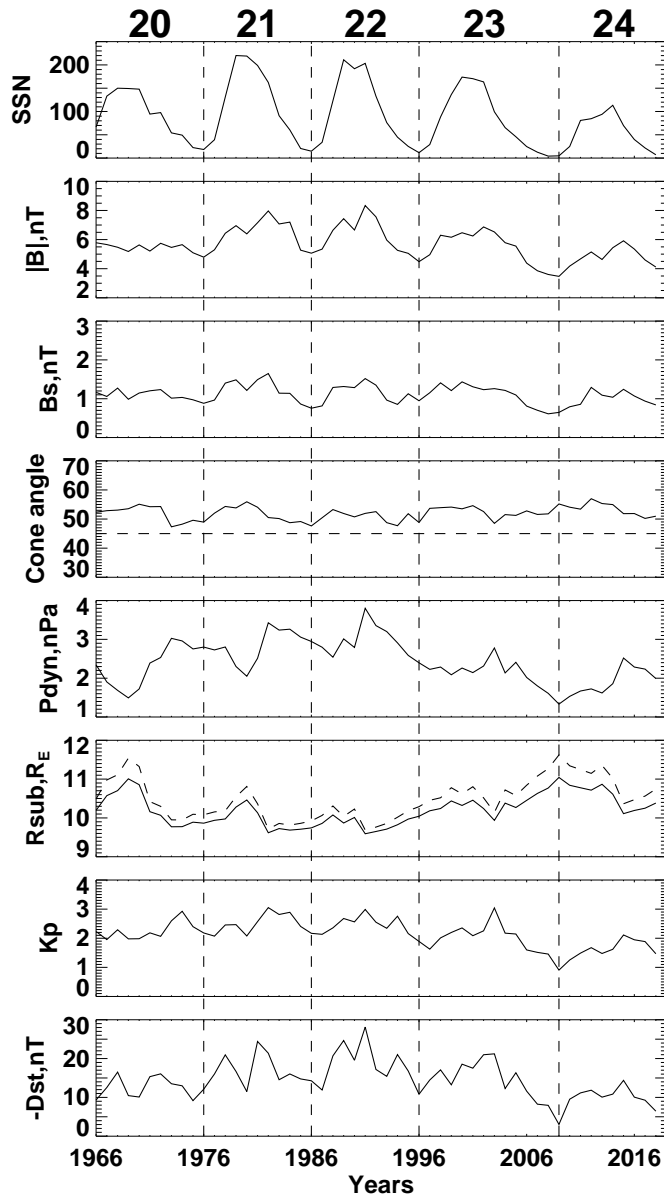


Figure 3. Expanded view of the annual average values from Fig. 2 (except for B_s and Kp). From the top, the sunspot numbers, IMF magnitude and average southward component B_s , IMF cone angle, solar wind dynamic pressure, magnetopause standoff distance (solid lines for Shue et al.'s model and dashed lines for Lin et al.'s model), Kp and Dst indices. Vertical lines separate solar cycles as indicated by numbers at the top.

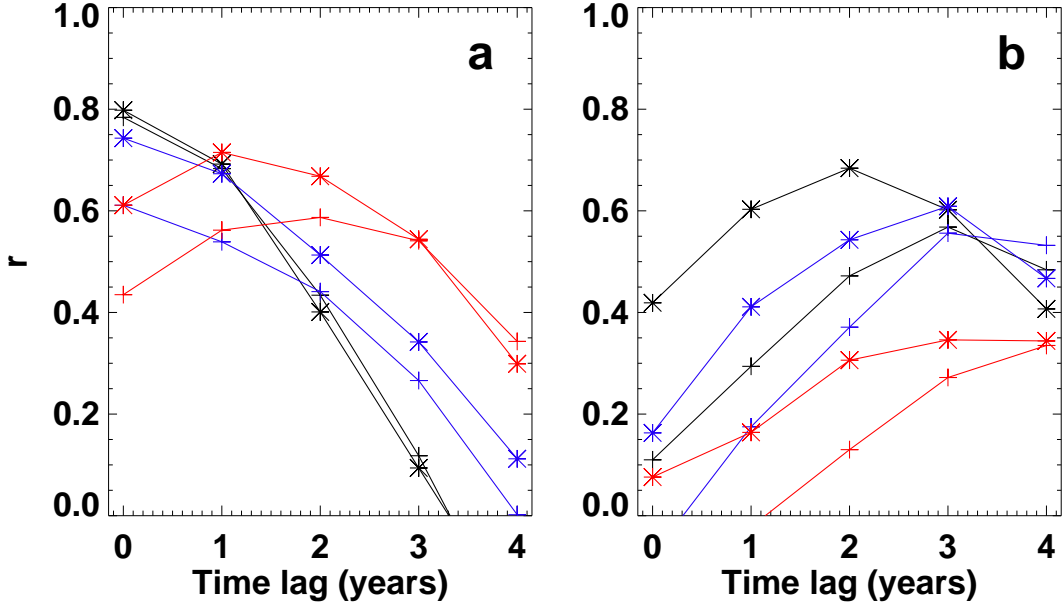


Figure 4. (a) The correlation coefficients between SSN and *Bs* (black), *Dst* (blue), and *Kp* (red) as a function of time lag for five (plus signs) and three (stars) solar cycles. (b) The correlation coefficients between SSN and *Pdyn* (black), *V* (blue), and *N* (red). Most correlations with coefficients below 0.3 are not statistically significant.

284 last three cycles taking 2 years time lag. This agrees with previous results, e.g. Köhnlein
 285 (1996) obtained a 2 year time lag between the SSN and solar wind velocity. Contrary
 286 to the correlation for 0 year time lag, the correlations coefficients for 1–4 year time lags
 287 correspond to p-values less than 0.05, i.e. they are statistically significant. However, (Crooker
 288 & Gringauz, 1993; Dmitriev et al., 2005) concluded that the dynamic pressure anticor-
 289 relates with the SSN analyzing mostly variations in cycles 20–21. If we consider sepa-
 290 rately the time interval between 1966 and 1986, we also find the anticorrelation between
 291 SSN and *Pdyn* with the coefficient of -0.51 (for zero time lag). Although this interval
 292 contains only 21 annual values, the correlation is statistically significant.

293 Since the correlations between the SSN and geomagnetic indices may also increase
 294 if taking into account a time lag (Echer et al., 2004), we calculate the correlations be-
 295 tween the annual SSN and *Bs*, *Kp*, and *Dst* for variable time lags from 0 to 4 years. As
 296 we note above, the correlation between SSN and *Pdyn* is higher for three last solar cy-
 297 cles, than for the whole 53-year interval, therefore we provide the coefficients for both
 298 the last five and three cycles. Figure 4 shows the results of calculations. The left panel
 299 shows the correlation coefficients for *Bs*, *Dst*, and *Kp*, while the right panel shows the
 300 coefficients for *Pdyn*, *V*, and *N*.

301 The correlation coefficients between SSN and *Bs*, and SSN and *Dst* are highest for
 302 a 0-year time lag. The correlation between SSN and *Kp* is highest for 2-year time lag
 303 (for five cycles) and for 1-year time lag (for three cycles). As mentioned above, the cor-
 304 relation between SSN and *Pdyn* is highest for 2–3 years time lag depending on the time
 305 interval. The correlation coefficient between SSN and *V* peaks for 3-year time lag in both
 306 cases. The density correlation with the solar activity is significantly worse than with other
 307 solar wind parameters. In fact, the only statistically significant correlation (according
 308 to our criterion) has been obtained for 4-year time lag and 5 solar cycles interval. In this
 309 case, the correlation coefficient grows up to only 0.33.

Table 2. Comparison of average solar wind and magnetospheric parameters in cycles 22 and 24. The magnetopause standoff distance is calculated by the L10 model. $\langle N_{22} \rangle$ and $\langle N_{24} \rangle$ are the average values for corresponding cycles, N_{09} and N_{91} are the average annual values in 2009 (minimum between 23rd and 24th cycles) and 1991 (maximum of 24th cycle) respectively. The bottom two rows are dimensionless.

	SSN	$ B , \text{nT}$	P_{dyn}, nPa	R_{sub}, R_E	Kp
$\langle N_{22} \rangle$	106.3	7.0	2.96	10.0	2.45
$\langle N_{24} \rangle$	53.6	5.3	1.87	11.0	1.57
$\langle N_{24} \rangle / \langle N_{22} \rangle$	0.50	0.76	0.63	1.10	0.64
N_{09}/N_{91}	0.024	0.42	0.35	1.20	0.30

310 Considering the whole 53-year interval in Figure 4, we note that the dynamic pres-
 311 sure increases until 1991 (except for the local minima in 1980 and 1990) and then fol-
 312 lows a decreasing trend between 1991 and 2009. It increases again in the present cycle
 313 untill 2015. The average annual values vary significantly, from 3.80 nPa in 1991 to 1.33
 314 nPa in 2009, i.e. by a factor of 3. Respectively, the average magnetopause standoff dis-
 315 tance varies between 9.59 R_E for the S98 model (9.68 R_E for the L10 model) in 1991 and
 316 11.04 R_E for the S98 model (11.62 R_E for the L10 model) in 2009. Thus the magnetopause
 317 models predict a 1.5–2 R_E variation in the standoff distance in the 17-years interval from
 318 the maximum of the 22nd to the minimum between the 23rd and 24th cycles.

319 In fact, the same decreasing trend after 1991 occurs for the other parameters in Fig-
 320 ure 4, i.e. for the SSN, $|B|$, and B_s . At the same time the Dst index increases ($-Dst$
 321 decreases) which may indicate both decrease in the average ring current and reduction
 322 in the magnetospheric compression (see discussion in Section 4). To emphasize this trend
 323 we draw the average solar wind and magnetospheric parameters for each solar cycle in
 324 Figure 5. In general, the trends for all of the parameters are very similar, taking into ac-
 325 count that the variations of R_{sub} are reversed to P_{dyn} . Both the average SSN and $|B|$
 326 have a maximum in the 21st cycle, while the solar wind dynamic pressure reaches its max-
 327 imum in the 22nd cycle. However, the differences for all these parameters between the
 328 21st and 22nd cycles are insignificant being smaller than the standard deviations. Kp
 329 has the maximum in the 21st cycle, and Dst in the 22nd cycle, but Kp in the 21st cy-
 330 cle is only 0.5% higher than in the 22nd cycle.

331 We quantify the differences between cycles 22 and 24 in Table 2. As follows from
 332 the table, the average P_{dyn} and Kp decrease by 37 % and 36 % respectively between
 333 cycles 22 and 24, and R_{sub} increases from 10.0 to 11.0 R_E , i.e. by 10 %. If we compare
 334 the years 1991 and 2009, P_{dyn} and Kp decrease by 65 % and 70 % respectively, while
 335 R_{sub} increases by 20 %. In particular, the values of R_{sub} according to the L10 model
 336 in 1991 and 2009 are 9.68 and 11.62 R_E respectively. Note that the R_{sub} in the L10 model
 337 varies with P_{dyn} according to a power-law index of only -0.19, however the annual dif-
 338 ference in the magnetopause position of about 2 R_E is significant and should be taken
 339 into account when preparing for the future space missions (as discussed in Section 4).

340 3 Extreme daily magnetopause distance

341 We further study the extreme solar wind conditions and identify the dates when
 342 the predicted magnetopause standoff distance is very small. We use the minimum daily
 343 average values shown by blue line in Figure 2. We take the L10 model which probably
 344 gives more realistic results for extreme solar wind and magnetospheric conditions (Dmitriev
 345 et al., 2016). Table 3 shows the dates and daily parameters for the events for which the

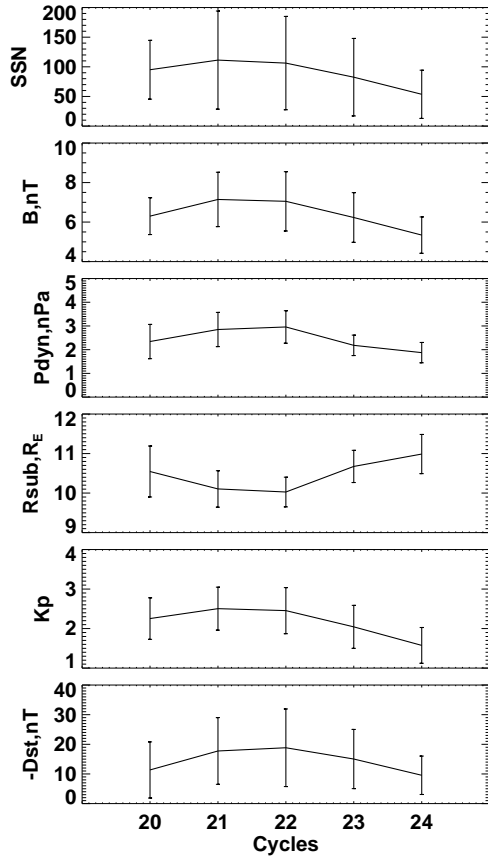


Figure 5. The sunspot numbers, IMF magnitude, solar wind dynamic pressure, magnetopause standoff distance in the L10 model, K_p and Dst indices averaged for each solar cycle. The error bars indicate standard deviations obtained from monthly values.

Table 3. The dates with daily minimal magnetopause distance according to the L10 model, the daily averages of P_{dyn} , B_z , and R_{sub} , average and minimal Dst , and average Kp .

	P_{dyn}, nPa	B_z, nT	R_{sub}, R_E	Dst	Dst_{min}	Kp
5 Jun 1991	20	-8.8	5.9	-147	-223	7.8
31 Mar 2001	14	-6.3	6.6	-211	-387	7.6
29 May 2003	17	-4.3	6.5	-46	-144	5.7

346 model predicts the daily magnetopause distance to be less than $6.62 R_E$, i.e. geosynchronous
347 magnetopause crossings (GMCs). We can find only three such days probably because
348 (1) the days with extreme solar wind conditions in the 20th and 21st cycles have large
349 data gaps and (2) the condition for daily average $R_{sub} < 6.62 R_E$ is very restrictive. The
350 average dynamic pressure is high, larger than 14 nPa, in all events, as expected. More-
351 over, the IMF B_z is strongly negative, which is the second reason for the decreasing of
352 the magnetopause standoff distance. The daily dynamic pressures and B_z in these events
353 match the necessary conditions for geosynchronous magnetopause crossings in Suvorova
354 et al. (2005).

355 The last two events in Table 3 are classified as CME-related in the ACE Richardson
356 and Cane catalogue (www.srl.caltech.edu/ACE/ASC/DATA/level3/icmetable2.htm)
357 and, moreover, are associated with the subsequent CMEs, suggesting that possibly com-
358 plex and interacting CMEs are causing the closest stand-off distance. The first event in
359 1991 seems to be also associated with a solar flare observed on 4 June and possibly CME-
360 related (Rank et al., 2001). The major magnetic storm of 4-5 June 1991 was studied by
361 Garner et al. (2004). All the events have minimum Dst below -100 nT, therefore may
362 be classified as magnetic storms, and Kp is 5.7 or higher.

363 We used 1-min averaged magnetic field data obtained from geosynchronous space-
364 craft GOES 8-13, and 15 to identify the GMC events with negative B_z . Only intervals
365 lasting more than five minutes have been selected and several events in one day have been
366 classified as one event. Figure 6 reproduces the minimum annual magnetopause stand-
367 off distance for the L10 model shown in Figure 2 superimposed by the histogram with
368 the number of days in each year when GOES observed negative B_z on the dayside (0600-
369 1800 MLT). The last two events in Table 3 are also included in this statistics.

370 The histogram covers the interval from 1996 to 2017, but the geosynchronous mag-
371 netopause crossings were observed only around the maximum of the 23rd cycle, from 1999
372 to 2006, and in 24th cycle from 2011 to 2014. Most of the crossings occur in 2000, 2001,
373 and 2003, when the model predicts drops in the minimal standoff distance. In general,
374 the anticorrelation between red and blue lines in Figure 6 seems to be good taking into
375 account that the blue line reflects only minimum average magnetopause distance in one
376 day, e.g. in one event, for each year. On the other hand, the red line may miss some GMC
377 events if there were no GOES measurements at the particular time in the dayside region
378 or GMCs were for positive B_z .

379 4 Discussion and Conclusions

380 This work investigates variations in the average magnetopause standoff distance
381 from 1966 to 2018 using OMNI data and empirical magnetopause models. According to
382 most empirical models, the standoff distance depends on the solar wind dynamic pres-
383 sure and IMF B_z (e.g., Shue et al. (1998)), but in addition to these two parameters it
384 may also depend on the solar wind magnetic pressure (Lin et al., 2010). Other param-
385 eters, such as the solar wind velocity (in addition to the dynamic pressure) or ionospheric

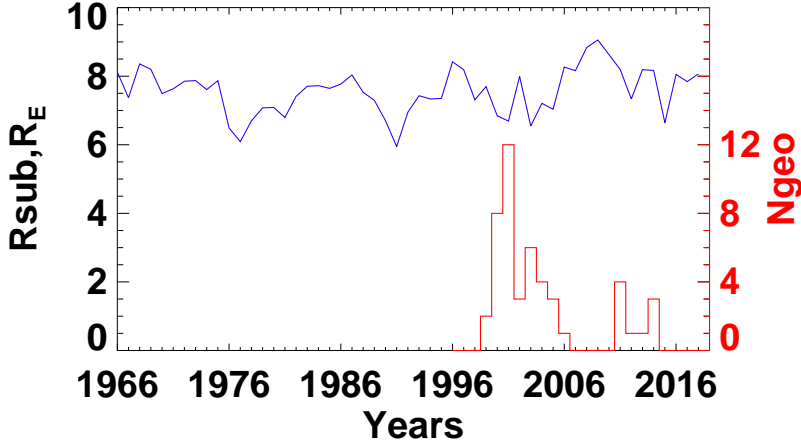


Figure 6. The annual minimal (blue) magnetopause standoff distance in the L10 model (the same as in Figure 2), and the number of days with negative B_z at geosynchronous orbit (red).

386 conductivity, may control the magnetospheric compression too (Němeček et al., 2016),
 387 but their influence is not yet firmly established. The ring current may also control the
 388 magnetopause standoff distance during geomagnetically disturbed conditions, especially
 389 in the main phase of magnetic storms (Dmitriev et al., 2016). Moreover, recent studies
 390 show that the magnetosphere may significantly expand during intervals with nearly radial
 391 IMF (Dušík et al., 2010; Grygorov et al., 2017; Park et al., 2016; Suvorova et al.,
 392 2010; Suvorova & Dmitriev, 2015), however this effect has not been incorporated in empirical
 393 models so far.

394 We use annual average and extreme solar wind and magnetospheric parameters in
 395 this work. On such a long timescale, the average IMF B_z approaches zero. The annual
 396 IMF cone angle varies in a narrow interval between 54.0° and 61.2° with the average of
 397 57.6° . Since a quasi-radial IMF orientation usually means small cone angles, e.g. less than
 398 or equal to 30° (Dušík et al., 2010), we think that quasi-radial intervals do not influence
 399 significantly our predictions of the magnetopause standoff distance on the annual time
 400 scale. As a result, the annual standoff distance depends mainly on the solar wind dynamic
 401 pressure. However, the power law indices of this dependence differ between the
 402 empirical models. For this reason, we have compared predictions of the two models, S98
 403 and L10. The second model predicts stronger variations with P_{dyn} and possibly better
 404 corresponds to observations even for disturbed magnetospheric conditions (Samsonov
 405 et al., 2016; Suvorova & Dmitriev, 2015).

406 We have calculated both the annual average standoff distance and extreme distances
 407 for each year. The extreme distances have been defined as minimum and maximum daily
 408 values. Both the minimum and maximum standoff distances vary with solar cycles in
 409 such a way that not only very compressed but also expanded subsolar magnetosphere
 410 can be observed near solar maximum, rather than just near solar minimum. The annual
 411 IMF magnitude (IMF B_z) correlate with sunspot numbers with the correlation coefficients
 412 0.75 (0.78) and a zero time lag. The annual average solar wind dynamic pressure
 413 correlates with the sunspot numbers with a coefficient of 0.57 if taking into account a
 414 time lag between P_{dyn} and SSN. We obtain a time lag of three years for the whole 53-
 415 year time interval. Considering only the three last cycles increases the correlation coefficient
 416 to 0.68 and gives a time lag of two years. The solar wind density poorly correlates
 417 with the SSN, the only statistically significant correlation occurs for a 4-year time lag
 418 and the correlation coefficient grows up to only 0.33. The solar wind velocity correlates
 419 with the SSN better than the density, and the correlation coefficient is equal to

0.56 (0.61 for three cycles) for a time lag of three years. Both the density and velocity do not correlate with the IMF B_z for a zero time lag, very poorly correlate with the IMF $|B|$, but significantly better anticorrelate with the IMF cone angle. The correlation coefficient between the cone angle and velocity (density) is equal to -0.61 (-0.51). The correlation is even higher between the cone angle and dynamic pressure. The reason of this anticorrelation is possibly differences in solar wind on a large time scale, i.e. fast and slow solar wind may correspond to slightly different average cone angles. However, a detailed study of this problem is out of scope of the paper.

The correlations between SSN and magnetospheric indices (Kp and Dst) are also higher for the last three cycles than for the whole time interval. Varying time lags, we obtain the highest correlation coefficients between SSN and B_s , and between SSN and Dst for a zero year time lag. The correlation coefficient between SSN and Kp peaks for 1–2 year time lag. In the whole interval, Kp better correlates with $Pdyn$ and $Rsub$ (with coefficients of about 0.8), while $-Dst$ better correlates with B_s (0.71) than with $Pdyn$ (0.63) or $Rsub$ (-0.58). At the same time, both Kp and $-Dst$ nicely correlate with the IMF magnitude with correlation coefficients above 0.8. Note that we use annual average values for these correlations and the results may differ from the correlations on shorter timescales. The correlations between solar wind parameters and magnetospheric indices were previously calculated mostly using hourly values. For example, Newell et al. (2007) obtained the correlation coefficients between Kp and B_s equal to -0.57, between Kp and $Pdyn$ equal to 0.51, between Dst and $Pdyn$ equal to -0.55 (but in their study Dst was corrected by adding an additional term proportional to $Pdyn^{1/2}$). Lockwood et al. (2019) noted that the correlation between solar wind parameters and magnetospheric indices is higher on a longer timescale. We think that the correlations between annual solar wind and magnetospheric parameters may reveal deeper relations between them than the correlations on shorter time scale, because we eliminate any uncertainty, e.g. in the time of magnetospheric response, and also remove the seasonal effects.

The Dst index is calculated as the deviation of the H component at mid-latitude stations from their quiet day values and is supposed to depend on variations of the ring current, magnetopause current, and to a lesser extent tail current (Burton et al., 1975) (see also the description of Dst at <http://wdc.kugi.kyoto-u.ac.jp>). An increase in the ring current decreases Dst , while an increase in the magnetopause current increases Dst . Solar wind dynamic pressure pulses may increase both the magnetopause and ring currents, however these increases occur on different time scales. The magnetopause current rapidly increases after the pressure pulse has reached the subsolar point. The ring current reacts on a much longer time scale. First, the solar wind energy flux into the magnetosphere increases due to the magnetopause reconnection, the energy is accumulated in the magnetotail and then released through energetic particles accelerated by magnetotail reconnection. Besides, the particles are also accelerated by the convective electric field which penetrates into the magnetosphere due to the magnetopause reconnection. Considering only the annual average parameters, we cannot detect a Dst response to short time scale variations in the magnetopause current, and mostly observe a long time scale response to the ring current. The last explains the correlation between annual $Pdyn$ and $-Dst$.

The average solar wind dynamic pressure exhibits increasing trend before 1991 and decreasing trend between 1991 and 2009. It increases again in the 24th cycle until 2015. The same trends have been observed in the SSN and average IMF. Respectively, the magnetopause standoff distance increases from 9.7 to 11.6 R_E (according to the L10 model) from 1991 to 2009. Later, it decreases to 10.4 R_E in 2015 and slightly increases again. In 2017, the standoff distance is 10.6 R_E (L10 model) and 10.2 (S98 model), and in 2018 the distance in the two models increases to 10.8 and 10.4 R_E , correspondingly. These standoff distances are close to the average values in the whole 53-years interval which equal 10.5 R_E (L10 model) and 10.2 R_E (S98 model). Meanwhile, the extreme daily stand-

473 off distances in 2018 (in the L10 model) equal 8.1 and 12.8 R_E respectively. The annual
 474 solar wind dynamic pressure decreases from 2.23 nPa in 2017 to 1.99 nPa in 2018. Note
 475 that in the three last solar minima the minimum of the dynamic pressure whether co-
 476 coincided with the solar minimum (between 23rd and 24th cycles) or was 2-3 years delayed
 477 (between 21st and 22nd, and between 22nd and 23rd) as shown in Figure 4. Now the
 478 solar activity is nearly at minimum, and we may expect keeping about the same low av-
 479 erage dynamic pressure for this year.

480 Lockwood et al. (2009) calculated solar wind parameters during the 20th century
 481 by reconstruction from geomagnetic activity data. They found that the solar wind ve-
 482 locity, IMF magnitude, and the open solar flux show a long-term increase during the first
 483 half of the 20th century followed by peaks around 1955 and 1986 and then a decrease.
 484 They predicted the end of the current grand solar maximum between 2013 and 2027 de-
 485 pending on the parameter considered. This generally agrees with the trends discussed
 486 in this paper. Our annual average results (Figure) also agree with Petrinec et al. (1991)
 487 who noted that the solar wind dynamic pressure was lower in 1979-1980 than during the
 488 following solar minimum between 21st and 22nd cycles. This might be related to spe-
 489 cific features of the 21st cycle in which a decrease of the open solar flux and solar wind
 490 speed appears right at SSN maximum in 1980 (Richardson et al., 2000). Furthermore,
 491 Dmitriev et al. (2009) concluded that the dynamic pressure anticorrelates with the SSN
 492 in the four solar cycles, from 20th to 23rd. Using the annual average values in our study,
 493 we confirm the anticorrelation between P_{dyn} and SSN in cycles 20–21, but get the cor-
 494 relation with the 2 years time lag in cycles 22-24. We note that even the annual mag-
 495 netospheric indices (Kp and Dst) as well as the IMF magnitude display no correlation
 496 with the SSN in cycle 20. We just point out this phenomenon here, but do not suggest
 497 any explanation.

498 Using our dataset, we have found dates when the predicted subsolar magnetopause
 499 was very close to the Earth. Because of many datagaps before 1995, we find only three
 500 daily values of R_{sub} smaller than the geostationary distance 6.62 (see Table 3). In all
 501 the events, the cause of the large magnetospheric compression seems to be related to CMEs,
 502 or, even, to CME series in at least two of the three events.

503 We suggest another way to check that the predictions of magnetopause distance
 504 with empirical models on a long timescale are reasonably good. We have compared the
 505 number of events with negative B_z at geosynchronous orbit and annual minimum mag-
 506 netopause distance between 1996 and 2018. We obtain that minima in the minimum R_{sub}
 507 nearly coincide with maxima on the histogram of negative B_z events although the two
 508 plots illustrate different processes. The minimum R_{sub} corresponds to a minimum stand-
 509 off distance in one event (possibly related to a strongest CME or a combination of CME-
 510 CME/CIR-CME in this year), while the number of negative B_z events may be roughly
 511 proportional to the number of most geoeffective CMEs (CME-CME or CIR-CME) in the
 512 year.

513 We summarize the main results below.

514 1. The average annual magnetopause standoff distance significantly changes dur-
 515 ing the last five solar cycles. In particular, the empirical models predict increase of the
 516 standoff distance by nearly 2 R_E from 1991 to 2009 which corresponds to a threefold de-
 517 crease of the solar wind dynamic pressure. This reflects a long-term decrease of the so-
 518 lar activity manifested also in the annual SSN, IMF magnitude, and magnetospheric Kp
 519 and Dst indices.

520 2. The annual southward IMF B_s correlates with SSN with a zero time lag, while
 521 the annual dynamic pressure correlates with SSN with 2–3 year time lag. The solar wind
 522 density poorly correlates with SSN, even taking into account the time lag, however the
 523 density and velocity are well anticorrelated with the IMF cone angle. The density bet-

524 ter correlates with the dynamic pressure than the velocity. The annual Kp better cor-
 525 relates with P_{dyn} , while Dst better correlates with B_s . Correspondingly, we obtain 1–
 526 2 years time lag for correlation between SSN and Kp , and a zero time lag between SSN
 527 and Dst . The time lags correspond to the maximum of the correlation coefficients.

528 3. We find an anticorrelation between the annual solar wind dynamic pressure and
 529 SSN in cycles 20–21 and a correlation in cycles 22–24.

530 4. The annual IMF cone angle weakly correlates with SSN and does not correlate
 531 with the IMF magnitude. The annual cone angle varies from 54.0° to 61.2° with aver-
 532 age of 57.6° .

533 5. We find extreme (minimal and maximal) solar wind parameters and magneto-
 534 spheric indices for each year, and their variations follow the solar cycles. We suggest that
 535 the extreme solar wind parameters often result from CMEs. We show that the three events
 536 with smallest daily magnetopause distance were related to CME impacts. At least in two
 537 of the three cases two successive CMEs were observed.

538 The knowledge of predicted magnetopause position for the next solar cycle is im-
 539 portant for future space missions, especially for those which are intended to observe the
 540 dayside magnetopause whether in situ or remotely. One of the forthcoming missions which
 541 will study variations of the dayside magnetopause is the Solar Wind Magnetosphere Ion-
 542 sphere Link Explorer (SMILE) (Raab et al., 2016).

543 Acknowledgments

544 The OMNI data are available from Coordinated Data Analysis Web (CDAWeb),
 545 <http://cdaweb.gsfc.nasa.gov>. GOES magnetic field data are available from CDAWeb
 546 and National Oceanic and Atmospheric Administration (NOAA), [http://ngdc.noaa](http://ngdc.noaa.gov)
 547 [.gov](http://ngdc.noaa.gov).

548 AAS and GBR acknowledge support from the UK Space Agency under grant ST/R002258/1.
 549 YVB was partly supported by the STFC RAL Space in-house research grant and by the
 550 NERC grant NE/P016863/1 'Space Weather Impacts on Ground-based Systems'. JS and
 551 ZN acknowledge support from the Czech Science Foundation under grant 17-06065S.

552 References

- 553 Aellig, M. R., Lazarus, A. J., & Steinberg, J. T. (2001). The solar wind helium
 554 abundance: Variation with wind speed and the solar cycle. *Geophys. Res.*
 555 *Let.*, *28*, 2767-2770. doi: 10.1029/2000GL012771
- 556 Borovsky, J. E., & Denton, M. H. (2006). Differences between cme-driven
 557 storms and cir-driven storms. *J. Geophys. Res.*, *111*(A7). doi: 10.1029/
 558 2005JA011447
- 559 Bothmer, V., & the EU-INTAS-ESA Team. (2004, Aug). The solar and interplan-
 560 etary causes of space storms in solar cycle 23. *IEEE Transactions on Plasma*
 561 *Science*, *32*(4), 1411-1414. doi: 10.1109/TPS.2004.830990
- 562 Burton, R. K., McPherron, R. L., & Russell, C. T. (1975). An empirical rela-
 563 tionship between interplanetary conditions and dst. *Journal of Geophys-*
 564 *ical Research (1896-1977)*, *80*(31), 4204-4214. Retrieved from [https://](https://agupubs.onlinelibrary.wiley.com/doi/abs/10.1029/JA080i031p04204)
 565 agupubs.onlinelibrary.wiley.com/doi/abs/10.1029/JA080i031p04204
 566 doi: 10.1029/JA080i031p04204
- 567 Crooker, N. U., & Gringauz, K. I. (1993). On the low correlation between long-term
 568 averages of solar wind speed and geomagnetic activity after 1976. *Journal of*
 569 *Geophysical Research: Space Physics*, *98*(A1), 59-62. Retrieved from [https://](https://agupubs.onlinelibrary.wiley.com/doi/abs/10.1029/92JA01978)
 570 agupubs.onlinelibrary.wiley.com/doi/abs/10.1029/92JA01978 doi: 10

- 571 .1029/92JA01978
- 572 Denton, M. H., Borovsky, J. E., Skoug, R. M., Thomsen, M. F., Lavraud, B., Hen-
- 573 derson, M. G., ... Liemohn, M. W. (2006). Geomagnetic storms driven
- 574 by icme- and cir-dominated solar wind. *J. Geophys. Res.*, *111*(A7). doi:
- 575 10.1029/2005JA011436
- 576 Dmitriev, A., Suvorova, A., & Chao, J.-K. (2011). A predictive model of geosyn-
- 577 chronous magnetopause crossings. *J. Geophys. Res.*, *116*, A05208. doi: 10
- 578 .1029/2010JA016208
- 579 Dmitriev, A. V., Lin, R. L., Liu, S. Q., & Suvorova, A. V. (2016). Model prediction
- 580 of geosynchronous magnetopause crossings. *Space Weather*, *14*(8), 530-543.
- 581 doi: 10.1002/2016SW001385
- 582 Dmitriev, A. V., Suvorova, A. V., Chao, J.-K., Wang, C. B., Rastaetter, L.,
- 583 Panasyuk, M. I., ... Myagkova, I. N. (2014). Anomalous dynamics of the
- 584 extremely compressed magnetosphere during 21 january 2005 magnetic storm.
- 585 *Journal of Geophysical Research: Space Physics*, *119*(2), 877-896. Retrieved
- 586 from [https://agupubs.onlinelibrary.wiley.com/doi/abs/10.1002/](https://agupubs.onlinelibrary.wiley.com/doi/abs/10.1002/2013JA019534)
- 587 [2013JA019534](https://agupubs.onlinelibrary.wiley.com/doi/abs/10.1002/2013JA019534) doi: 10.1002/2013JA019534
- 588 Dmitriev, A. V., Suvorova, A. V., & Veselovsky, I. S. (2009). Statistical character-
- 589 istics of the heliospheric plasma and magnetic field at the earth's orbit during
- 590 four solar cycles 20-23. In H. E. Johannson (Ed.), *Handbook on solar wind: Effects, dynamics and interactions* (p. 81-144). New York: NOVA Science
- 591 Publishers.
- 592
- 593 Dmitriev, A. V., Veselovsky, I. S., & Suvorova, A. V. (2005). Comparison of helio-
- 594 spheric conditions near the earth during four recent solar maxima. *Advances in*
- 595 *Space Research*, *36*, 2339-2344. doi: 10.1016/j.asr.2004.06.018
- 596 Dušík, v., Granko, G., Šafránková, J., Němeček, Z., & Jelínek, K. (2010). Imf cone
- 597 angle control of the magnetopause location: Statistical study. *Geophysical*
- 598 *Research Letters*, *37*(19). Retrieved from [https://agupubs.onlinelibrary](https://agupubs.onlinelibrary.wiley.com/doi/abs/10.1029/2010GL044965)
- 599 [.wiley.com/doi/abs/10.1029/2010GL044965](https://agupubs.onlinelibrary.wiley.com/doi/abs/10.1029/2010GL044965) doi: 10.1029/2010GL044965
- 600 Echer, E., Gonzalez, W. D., Gonzalez, A. L. C., Prestes, A., Vieira, L. E. A., dal
- 601 Lago, A., ... Schuch, N. J. (2004). Long-term correlation between solar and
- 602 geomagnetic activity. *Journal of Atmospheric and Solar-Terrestrial Physics*,
- 603 *66*, 1019-1025. doi: 10.1016/j.jastp.2004.03.011
- 604 Feynman, J. (1982). Geomagnetic and solar wind cycles, 1900-1975. *J. Geophys.*
- 605 *Res.*, *87*, 6153-6162. doi: 10.1029/JA087iA08p06153
- 606 Garner, T. W., Wolf, R. A., Spiro, R. W., Burke, W. J., Fejer, B. G., Sazykin, S.,
- 607 ... Hairston, M. R. (2004). Magnetospheric electric fields and plasma sheet
- 608 injection to low l-shells during the 4-5 june 1991 magnetic storm: Compari-
- 609 son between the rice convection model and observations. *J. Geophys. Res.*,
- 610 *109*(A2). doi: 10.1029/2003JA010208
- 611 Gleissberg, W. (1965). The eighty-year solar cycle in auroral frequency numbers. *J.*
- 612 *Br. Astron. Assoc.*, *75*, 227-231.
- 613 Gonzalez, W. D., Gonzalez, A. L. C., & Tsurutani, B. T. (1990). Dual-peak solar
- 614 cycle distribution of intense geomagnetic storms. *Planetary and Space Science*,
- 615 *38*(2), 181 - 187. doi: 10.1016/0032-0633(90)90082-2
- 616 Gopalswamy, N. (2006). Coronal mass ejections of solar cycle 23. *Journal of Astro-*
- 617 *physics and Astronomy*, *27*(2), 243-254. doi: 10.1007/BF02702527
- 618 Gopalswamy, N. (2008). Solar connections of geoeffective magnetic structures. *Jour-*
- 619 *nal of Atmospheric and Solar-Terrestrial Physics*, *70*, 2078-2100. doi: 10.1016/
- 620 [j.jastp.2008.06.010](https://doi.org/10.1016/j.jastp.2008.06.010)
- 621 Gosling, J. T., Bame, S. J., McComas, D. J., & Phillips, J. L. (1990). Coronal mass
- 622 ejections and large geomagnetic storms. *Geophysical Research Letters*, *17*(7),
- 623 901-904. doi: 10.1029/GL017i007p00901
- 624 Grygorov, K., Šafránková, J., Němeček, Z., Pi, G., Přech, L., & Urbář, J. (2017,
- 625 November). Shape of the equatorial magnetopause affected by the radial in-

- 626 terplanetary magnetic field. *Planetary and Space Science*, *148*, 28-34. doi:
627 10.1016/j.pss.2017.09.011
- 628 Hirshberg, J. (1973, February). The solar wind cycle, the sunspot cycle, and the
629 corona. *Astrophys. Space Sci.*, *20*, 473-481. doi: 10.1007/BF00642216
- 630 Janardhan, P., Bisoi, S. K., Ananthakrishnan, S., Tokumaru, M., Fujiki, K., Jose,
631 L., & Sridharan, R. (2015, July). A 20 year decline in solar photospheric
632 magnetic fields: Inner-heliospheric signatures and possible implications.
633 *Journal of Geophysical Research (Space Physics)*, *120*, 5306-5317. doi:
634 10.1002/2015JA021123
- 635 Jelínek, K., Němeček, Z., Šafránková, J., Shue, J.-H., Suvorova, A. V., & Sibeck,
636 D. G. (2010). Thin magnetosheath as a consequence of the magnetopause
637 deformation: Themis observations. *Journal of Geophysical Research: Space*
638 *Physics*, *115*(A10). Retrieved from [https://agupubs.onlinelibrary.wiley](https://agupubs.onlinelibrary.wiley.com/doi/abs/10.1029/2010JA015345)
639 [.com/doi/abs/10.1029/2010JA015345](https://agupubs.onlinelibrary.wiley.com/doi/abs/10.1029/2010JA015345) doi: 10.1029/2010JA015345
- 640 Kilpua, E. K. J., Luhmann, J. G., Jian, L. K., Russell, C. T., & Li, Y. (2014). Why
641 have geomagnetic storms been so weak during the recent solar minimum and
642 the rising phase of cycle 24? *Journal of Atmospheric and Solar-Terrestrial*
643 *Physics*, *107*, 12-19. doi: 10.1016/j.jastp.2013.11.001
- 644 King, J. H. (1979). Solar cycle variations in IMF intensity. *Journal of Geo-*
645 *physical Research: Space Physics*, *84*(A10), 5938-5940. doi: 10.1029/
646 JA084iA10p05938
- 647 Köhnlein, W. (1996). Cross-correlation of solar wind parameters with sunspots
648 ('long-term variations') at 1 au during cycles 21 and 22. *Astrophysics and*
649 *Space Science*, *245*(1), 81-88. doi: 10.1007/BF00637804
- 650 Kuznetsov, S. N., & Suvorova, A. V. (1998). An Empirical Model of the Magne-
651 topause for Broad Ranges of Solar Wind Pressure and B_z IMF. In J. Moen,
652 A. Egeland, & M. Lockwood (Eds.), *Polar cap boundary phenomena* (p. 51).
- 653 Lin, R. L., Zhang, X. X., Liu, S. Q., Wang, Y. L., & Gong, J. C. (2010). A three-
654 dimensional asymmetric magnetopause model. *Journal of Geophysical Research*
655 *(Space Physics)*, *115*, A04207. doi: 10.1029/2009JA014235
- 656 Link, F. (1962). Observations et catalogue des aurores boreales apparues en occident
657 de 626 a 1600. *Geofys. Sb.*, 297-387.
- 658 Liu, Y. D., Hu, H., Wang, R., Yang, Z., Zhu, B., Liu, Y. A., ... Richardson, J. D.
659 (2015). Plasma and magnetic field characteristics of solar coronal mass ejec-
660 tions in relation to geomagnetic storm intensity and variability. *Astrophys. J.*
661 *Lett.*, *809*(2), L34.
- 662 Lockwood, M., Bentley, S. N., Owens, M. J., Barnard, L. A., Scott, C. J., Watt,
663 C. E., & Allanson, O. (2019). The development of a space climatology: 1.
664 solar wind magnetosphere coupling as a function of timescale and the effect
665 of data gaps. *Space Weather*, *17*(1), 133-156. Retrieved from [https://](https://agupubs.onlinelibrary.wiley.com/doi/abs/10.1029/2018SW001856)
666 agupubs.onlinelibrary.wiley.com/doi/abs/10.1029/2018SW001856 doi:
667 10.1029/2018SW001856
- 668 Lockwood, M., Rouillard, A. P., & Finch, I. D. (2009). The rise and fall of open so-
669 lar flux during the current grand solar maximum. *Astrophys. J.*, *700*, 937-944.
670 doi: 10.1088/0004-637X/700/2/937
- 671 Lugaz, N., Temmer, M., Wang, Y., & Farrugia, C. J. (2017). The interaction of suc-
672 cessive coronal mass ejections: A review. *Solar Physics*, *292*(4), 64. doi: 10
673 .1007/s11207-017-1091-6
- 674 Luhmann, J. G., Lee, C. O., Li, Y., Arge, C. N., Galvin, A. B., Simunac, K., ...
675 Petrie, G. (2009). Solar wind sources in the late declining phase of cycle 23:
676 Effects of the weak solar polar field on high speed streams. *Solar Physics*,
677 *256*(1), 285-305. doi: 10.1007/s11207-009-9354-5
- 678 McComas, D. J., Angold, N., Elliott, H. A., Livadiotis, G., Schwadron, N. A., Sk-
679 oug, R. M., & Smith, C. W. (2013). Weakest Solar Wind of the Space
680 Age and the Current "Mini" Solar Maximum. *Astrophys. J.*, *779*, 2. doi:

- 681 10.1088/0004-637X/779/1/2
682 Merka, J., Szabo, A., Šafránková, J., & Němeček, Z. (2003). Earth's bow shock and
683 magnetopause in the case of a field-aligned upstream flow: Observation and
684 model comparison. *Journal of Geophysical Research: Space Physics*, 108(A7).
685 Retrieved from [https://agupubs.onlinelibrary.wiley.com/doi/abs/](https://agupubs.onlinelibrary.wiley.com/doi/abs/10.1029/2002JA009697)
686 10.1029/2002JA009697 doi: 10.1029/2002JA009697
687 Neugebauer, M. (1981). Observations of solar-wind helium. *Fundam. Cosmic. Phys.*,
688 7, 131-199.
689 Newell, P. T., Sotirelis, T., Liou, K., Meng, C.-I., & Rich, F. J. (2007). A
690 nearly universal solar wind-magnetosphere coupling function inferred from
691 10 magnetospheric state variables. *J. Geophys. Res.*, 112(A1). doi:
692 10.1029/2006JA012015
693 Němeček, Z., Šafránková, J., Lopez, R. E., Dušík, Š., Nouzák, L., Přech, L., ...
694 Shue, J.-H. (2016). Solar cycle variations of magnetopause locations. *Advances*
695 *in Space Research*, 58, 240-248. doi: 10.1016/j.asr.2015.10.012
696 Oh, S. Y., Yi, Y., & Kim, Y. H. (2007). Solar cycle variation of the interplanetary
697 forward shock drivers observed at 1 au. *Solar Physics*, 245(2), 391-410. doi:
698 10.1007/s11207-007-9042-2
699 Park, J.-S., Shue, J.-H., Kim, K.-H., Pi, G., Němeček, Z., & Šafránková, J. (2016).
700 Global expansion of the dayside magnetopause for long-duration radial
701 imf events: Statistical study on goes observations. *Journal of Geophysi-*
702 *cal Research: Space Physics*, 121(7), 6480-6492. Retrieved from [https://](https://agupubs.onlinelibrary.wiley.com/doi/abs/10.1002/2016JA022772)
703 agupubs.onlinelibrary.wiley.com/doi/abs/10.1002/2016JA022772 doi:
704 10.1002/2016JA022772
705 Petrinec, S. M., & Russell, C. T. (1996). Near-Earth magnetotail shape and size as
706 determined from the magnetopause flaring angle. *J. Geophys. Res.*, 101, 137-
707 152. doi: 10.1029/95JA02834
708 Petrinec, S. P., Song, P., & Russell, C. T. (1991). Solar cycle variations in the size
709 and shape of the magnetopause. *J. Geophys. Res.*, 96, 7893-7896. doi: 10
710 .1029/90JA02566
711 Press, W. H., Teukolsky, S. A., Vetterling, W. T., & Flannery, B. P. (1992). *Numer-*
712 *ical Recipes in C*. Cambridge: Cambridge University Press.
713 Pudovkin, M. I., Besser, B. P., & Zaitseva, S. A. (1998). Magnetopause stand-off dis-
714 tance in dependence on the magnetosheath and solar wind parameters. *Ann.*
715 *Geophys.*, 16, 388-396. doi: 10.1007/s00585-998-0388-z
716 Raab, W., Branduardi-Raymont, G., Dai, L., Wang, C., Donovan, E., Enno, G., ...
717 Zheng, J. (2016). Smile: a joint esa/cas mission to investigate the interac-
718 tion between the solar wind and earth's magnetosphere. In *Space telescopes*
719 *and instrumentation 2016: Ultraviolet to gamma ray* (Vol. 9905, p. 990502).
720 Retrieved from <http://oro.open.ac.uk/46941/>
721 Rank, G., Ryan, J., Debrunner, H., McConnell, M., & Schönfelder, V. (2001). Ex-
722 tended gamma-ray emission of the solar flares in june 1991. *Astronomy and*
723 *Astrophysics*, 378, 1046-1066. doi: 10.1051/0004-6361:20011060
724 Richardson, I. G., Cliver, E. W., & Cane, H. V. (2000). Sources of geomagnetic
725 activity over the solar cycle: Relative importance of coronal mass ejections,
726 high-speed streams, and slow solar wind. *J. Geophys. Res.*, 105(A8), 18203-
727 18213. doi: 10.1029/1999JA000400
728 Roelof, E. C., & Sibeck, D. G. (1993). Magnetopause shape as a bivariate function
729 of interplanetary magnetic field B_z and solar wind dynamic pressure. *J. Geo-*
730 *phys. Res.*, 98, 21. doi: 10.1029/93JA02362
731 Rouillard, A. P., Lockwood, M., & Finch, I. (2007). Centennial changes in the solar
732 wind speed and in the open solar flux. *J. Geophys. Res.*, 112, A05103. doi: 10
733 .1029/2006JA012130
734 Samsonov, A. A., Gordeev, E., Tsyganenko, N. A., Šafránková, J., Němeček, Z.,
735 Šimunek, J., ... Raeder, J. (2016). Do we know the actual magnetopause

- 736 position for typical solar wind conditions? *J. Geophys. Res.*, *121*, 6493-6508.
 737 doi: 10.1002/2016JA022471
- 738 Samsonov, A. A., Němeček, Z., Šafránková, J., & Jelínek, K. (2012). Why
 739 does the subsolar magnetopause move sunward for radial interplanetary
 740 magnetic field? *J. Geophys. Res.*, *117*(A5). Retrieved from [https://](https://agupubs.onlinelibrary.wiley.com/doi/abs/10.1029/2011JA017429)
 741 agupubs.onlinelibrary.wiley.com/doi/abs/10.1029/2011JA017429 doi:
 742 10.1029/2011JA017429
- 743 Samsonov, A. A., Sibeck, D. G., Šafránková, J., Němeček, Z., & Shue, J.-H. (2017).
 744 A method to predict magnetopause expansion in radial imf events by mhd
 745 simulations. *Journal of Geophysical Research: Space Physics*, *122*(3), 3110-
 746 3126. Retrieved from [https://agupubs.onlinelibrary.wiley.com/doi/abs/](https://agupubs.onlinelibrary.wiley.com/doi/abs/10.1002/2016JA023301)
 747 [10.1002/2016JA023301](https://agupubs.onlinelibrary.wiley.com/doi/abs/10.1002/2016JA023301) doi: 10.1002/2016JA023301
- 748 Shue, J.-H., Song, P., Russell, C. T., Steinberg, J. T., Chao, J. K., Zastenker, G.,
 749 ... Kawano, H. (1998). Magnetopause location under extreme solar wind
 750 conditions. *J. Geophys. Res.*, *103*, 17691-17700. doi: 10.1029/98JA01103
- 751 Siscoe, G. L. (1980). Evidence in the auroral record for secular solar vari-
 752 ability. *Reviews of Geophysics and Space Physics*, *18*, 647-658. doi:
 753 10.1029/RG018i003p00647
- 754 Siscoe, G. L., Crooker, N. U., & Christopher, L. (1978). A solar cycle variation of
 755 the interplanetary magnetic field. *Solar Phys.*, *56*, 449-461. doi: 10.1007/
 756 BF00152484
- 757 Suvorova, A., Dmitriev, A., Chao, J.-K., Thomsen, M., & Yang, Y.-H. (2005). Nec-
 758 essary conditions for geosynchronous magnetopause crossings. *J. Geophys.*
 759 *Res.*, *110*(A1). Retrieved from [https://agupubs.onlinelibrary.wiley.com/](https://agupubs.onlinelibrary.wiley.com/doi/abs/10.1029/2003JA010079)
 760 [doi/abs/10.1029/2003JA010079](https://agupubs.onlinelibrary.wiley.com/doi/abs/10.1029/2003JA010079) doi: 10.1029/2003JA010079
- 761 Suvorova, A. V., & Dmitriev, A. V. (2015). Magnetopause inflation under radial imf:
 762 Comparison of models. *Earth and Space Science*, *2*(4), 107-114. doi: 10.1002/
 763 2014EA000084
- 764 Suvorova, A. V., Shue, J.-H., Dmitriev, A. V., Sibeck, D. G., McFadden, J. P.,
 765 Hasegawa, H., ... Němeček, Z. (2010). Magnetopause expansions for quasi-
 766 radial interplanetary magnetic field: Themis and geotail observations. *J.*
 767 *Geophys. Res.*, *115*(A10). Retrieved from [https://agupubs.onlinelibrary](https://agupubs.onlinelibrary.wiley.com/doi/abs/10.1029/2010JA015404)
 768 [.wiley.com/doi/abs/10.1029/2010JA015404](https://agupubs.onlinelibrary.wiley.com/doi/abs/10.1029/2010JA015404) doi: 10.1029/2010JA015404
- 769 Yashiro, S., Gopalswamy, N., Michalek, G., St. Cyr, O. C., Plunkett, S. P., Rich,
 770 N. B., & Howard, R. A. (2004). A catalog of white light coronal mass
 771 ejections observed by the soho spacecraft. *J. Geophys. Res.*, *109*(A7). doi:
 772 10.1029/2003JA010282
- 773 Zerbo, J.-L., Amory-Mazaudier, C., & Ouattara, F. (2013). Geomagnetism during
 774 solar cycle 23: Characteristics. *Journal of Advanced Research*, *4*, 265-274. doi:
 775 10.1016/j.jare.2012.08.010
- 776 Zerbo, J.-L., & Richardson, J. D. (2015). The solar wind during current and
 777 past solar minima and maxima. *J. Geophys. Res.*, *120*(A9), 10. doi:
 778 10.1002/2015JA021407